


Article

# Enabling Complex Impedance Spectroscopy for Cardio-Respiratory Monitoring with Wearable Biosensors: A Case Study

R. Joseph Mathews\* and Emil Jovanov 

Department of Electrical and Computer Engineering, The University of Alabama in Huntsville, Huntsville, AL 35899, USA

\* Correspondence: rm0146@uah.edu

**Abstract:** Recent advances in commercially available integrated complex impedance spectroscopy controllers have brought rapid increases in the quality of systems available to researchers for wearable and remote patient monitoring applications. As a result, novel sensing methods and electrode configurations are increasingly viable, particularly for low-power embedded sensors and controllers for general electrochemical analysis. This study evaluates a case study of the four electrode locations suitable for wearable monitoring of respiratory and heart activity monitoring using complex impedance spectroscopy. We use tetrapolar electrode configurations with ten stimulation frequencies to characterize the relative differences in measurement sensitivity. Measurements are performed and compared for the magnitude, phase, resistive, and reactive components of the bioimpedance using two COTS-based controllers, the TI AFE4300 and MAX30009. We identify the highest percent relative changes in the magnitude of the impedance corresponding to deep breathing and heart activity across the chest (17% at 64 kHz, 0.5% at 256 kHz, respectively), on the forearm (0.098% at 16 kHz, 0.04% at 8 kHz), wrist-to-wrist across the body (0.28% at 256 kHz, 0.04% at 256 kHz, respectively), and wrist-to-finger across the body (0.35% at 4 kHz, 0.05% at 4 kHz, respectively). We demonstrate that the wrist-to-wrist and wrist-to-finger configurations are most promising and may enable new wearable bioimpedance applications. Additionally, this paper demonstrates that deep respiration and heart activity influence bioimpedance measurements in whole-body measurement configurations, with variations of nearly 1% in measured impedance due to the phase of the breathing cycle.

**Keywords:** wearable sensors; wearable monitoring; respiration monitoring; heart activity monitoring; bioimpedance spectroscopy; impedance pneumography; remote patient monitoring



check for updates

**Citation:** Mathews, R.J.; Jovanov, E. Enabling Complex Impedance Spectroscopy for Cardio-Respiratory Monitoring with Wearable Biosensors: A Case Study. *Electrochem* **2023**, *4*, 389–410. <https://doi.org/10.3390/electrochem4030025>

Academic Editors: Masato Sone and Gyöző G. Lang

Received: 14 March 2023

Revised: 7 June 2023

Accepted: 8 August 2023

Published: 10 August 2023



**Copyright:** © 2023 by the authors. Licensee MDPI, Basel, Switzerland. This article is an open access article distributed under the terms and conditions of the Creative Commons Attribution (CC BY) license (<https://creativecommons.org/licenses/by/4.0/>).

## 1. Introduction

The measurement of complex bioimpedance (BioZ) is a low-cost, non-invasive method for measuring the properties of biological tissues. An active area of research, the applications of bioimpedance measurements are numerous, from body composition [1,2], assessing the hydration status of athletes [3,4] and dialysis patients [5,6], to monitoring the volume of blood pumped with each heartbeat in heart failure patients [7,8]. Bioimpedance refers to measuring the properties of tissue by injecting a sinusoidal current at some frequency into the tissue and measuring the voltage difference between two points on the body. In a four-electrode or tetrapolar configuration, the current is injected through one electrode (the current source) and passes through the tissue to another electrode (the current sink). Between these two current electrodes, two voltage sense (differential) electrodes are placed. The positive voltage electrode is typically placed near the current source, while the negative voltage electrode is typically placed near the current sink. A typical example is a body composition measurement with a device such as the Impedimed SFB7 [9], with four segments acting as a current source, sink, and differential input. In a bipolar configuration, the current source and positive voltage sense are connected to the same electrode, while

the current sink and negative voltage sense are connected to the other electrode. While the bipolar configuration is simpler, it has the disadvantage of including the electrode–tissue interface impedance in series with the tissue under study. Further complicating matters, the electrode–skin interface impedance changes with frequency. For this reason, the tetrapolar configuration is often used for more accurate measurements, though mismatches in the electrode–skin impedance can still cause errors [10]. Depending on the application, these electrodes may be placed in any number of locations across the body.

In this paper, measurement configurations and frequencies suitable for real-time wearable BioZ monitoring are evaluated. Typical applications with smart clothes and smartwatches motivated our focus on chest measurements for a direct measurement of heart/lungs, as well as forearm and wrist (unilateral and bilateral) BioZ monitoring. To determine the dynamic response of the tissues, the relative change of the complex bioimpedance (magnitude, phase, real/imaginary) was evaluated as a function of body location, measurement setup, and stimulus frequency for changes resulting from respiration and heart activity. This study uses novel electrode configurations and a wide range of frequencies to investigate the possibility of real-time cardiorespiratory monitoring in a wrist-watch- or clothing-based bioimpedance system. Such a system could enable at-home monitoring of heart and lung diseases and empower primary care providers with additional data on treatment effects. We believe that the results of this comparative site evaluation might guide the design of wearable monitors and implementation of real-time monitoring applications.

There are two broad classes of BioImpedance Analysis (BIA): assessment of the frequency-domain response of the tissue, and monitoring of the time-domain response. Most applications, such as body composition analysis, will use multiple, discrete frequencies (called multiple-frequency BIA (MF-BIA) or bioimpedance spectroscopy (BIS)) in succession in a short span of time to characterize the frequency response of the tissues at different frequencies, typically ranging from single kHz to approximately one MHz. Commercially available devices such as the Impedimed SFB7 [9] use a frequency sweep of 256 logarithmically spaced frequencies between 1 kHz and 1 MHz in less than one second to collect this response. Applications such as impedance cardiography or pneumography often continuously measure a Single Frequency (SF-BIA) at a high sample rate for a set time period to obtain the changing response of the tissue between the electrodes due to respiration or heart activity. Many single-frequency applications use 50 kHz [11,12] as a stimulus frequency, as there are contributions from both intracellular and extracellular water at this frequency [13]. Frequencies higher than 100 kHz are less common for single frequency applications because of parasitic capacitance at higher frequencies [14] as well as frequency limitations of the Commercial off-the-shelf (COTS) front ends (e.g., Texas Instruments AFE4300 in IQ mode is limited to 64 kHz [15]). Many studies use one or a combination of the magnitude, phase, real (resistive), and imaginary (reactive) components of impedance [3,16] to evaluate and compare tissue properties.

Advances in integrated circuits have greatly benefited bioimpedance monitoring systems, making them smaller, cheaper, more sensitive, and easier to use [17]. COTS controllers on the market from Texas Instruments, Analog Devices, and MAXIM feature sensitivity and accuracy of the high-end systems from twenty years ago, while priced under ten dollars. A recent study [18] found the MAXIM MAX30009 [19], used in this paper, compares favorably with a Zurich Instruments High Precision Multi-Frequency Impedance Analyzer [20], USD 12,260 at time of publication, in the 1 kHz to 300 kHz range. Bioimpedance controllers such as this and similar offerings by competitors bring improved range and sensitivity, as well as reduced power consumption to wearable device designers. Moreover, their size and power consumption make them suitable for real-time wearable monitoring applications and remote patient monitoring. Previously published research projects were limited by the hardware (frequency, sensitivity, I vs. Q, etc.), and would certainly benefit from faster sweeps, increased frequency ranges, higher sample rates, and increased resolution offered by the latest generation of integrated controllers.

The COVID-19 pandemic especially emphasized the need for effective triage and at-home monitoring using wearable monitors [21]. Researchers in the wearable health monitoring and remote patient monitoring area have used bioimpedance technology in several broad research avenues, such as heart health monitoring, where specific applications include cuff-less blood pressure monitoring [22], non-invasive heart rate variability [23], heart stroke volume estimation [7], and respiration monitoring [24,25], where specific applications include lung volume measurement [26] and respiration rate monitoring [27]. Smart clothes and accessories provide an opportunity for the seamless embedding of the embedded controllers, electrodes, and interconnections necessary for real-time wearable BIA. Wearable physiological monitoring is particularly important for users with chronic conditions [28,29]. People with three or more chronic conditions (28% of the population) account for 67% of total healthcare expenditures in the United States, and over 80% of people over 65 have multiple chronic conditions [30]. Many of these chronic conditions are heart and lung conditions [31]. Roughly 1 in 4 US adults suffer from hypertension, and 1 in 12 from upper respiratory conditions [30]. With an aging population and high incidences of heart and lung disease, there has been a continually rising increase in interest in systems that can provide monitoring capabilities for these conditions, especially at home [32]. We believe that the electrode configurations and frequencies studied may be appropriate for future wearable applications to address these needs.

This paper is structured as follows: Section 1 contains the introduction; Section 2, materials and methods, describes the measurement setup, the rationale for measurement locations, subjects, etc.; Section 3 presents the results; Section 4 discusses the results and provides the conclusions.

## 2. Materials and Methods

This section describes the measurement setup, equipment, and protocols used in the evaluation of configurations and setups suitable for wearable real-time BioZ monitoring.

### 2.1. Measurement Setup

The main candidate locations for the wearable BioZ monitoring evaluated are illustrated in Figure 1:

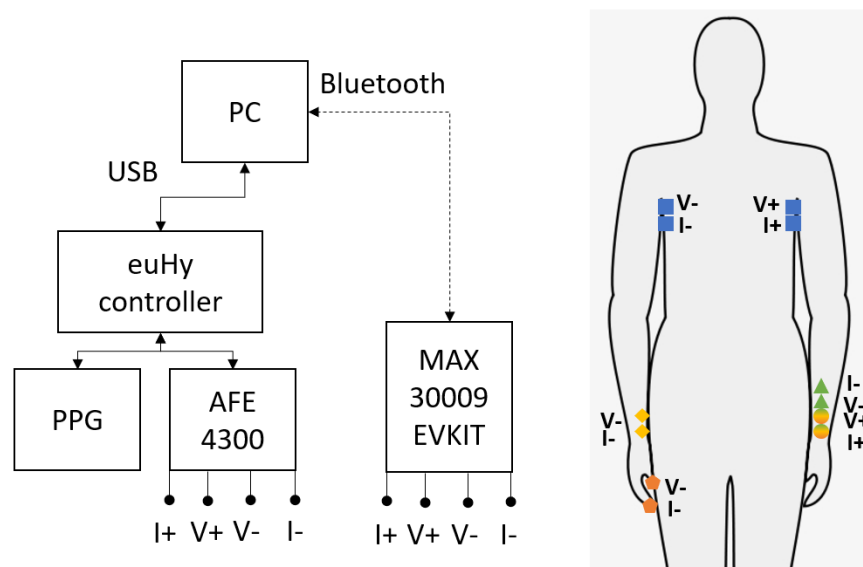


**Figure 1.** A visual representation of the system block diagram (left) and the electrode configurations (right). Note that the electrodes on the wrist on the right side of the figure closest to the hand labeled V+ and I+ are used as the source electrodes for the forearm, wrist-to-wrist, and wrist-to-fingers electrode configurations.

- Chest (Thoracic, blue, square)
- Forearm (unilateral, green, circle to triangle)
- Wrist-to-Wrist (bilateral, yellow, circle to diamond)
- Wrist-to-Finger (bilateral, orange, circle to pentagon)

All candidate locations are evaluated with the same set of sensors and protocols, which allows analysis of their suitability for different wearable applications. The well-studied chest configuration is used in many impedance cardiography and pneumography applications, and it is used in this paper as the baseline measurement. All of the following measurements are performed with the subject in a seated position, with both feet on the floor and both hands placed palms up in a comfortable resting position.

## 2.2. Measurement Location Rationale

There are many combinations of possible electrode locations and stimulation frequencies on the body, and to complicate matters further, the changes in the components of the measured impedance vary greatly with the location of electrodes/tissue under electrodes. Many researchers evaluate a single frequency (often 50 kHz [11], though 10–100 kHz is common) for multiple locations, or multiple frequencies at a single location. In this paper, both multiple frequencies and multiple locations are studied to comparatively evaluate site quality for physiological monitoring, primarily respiration, and heart activity. Therefore, it is important to establish baseline measurements for comparison with other works. Here, the chest configuration is used as the primary reference, and the forearm configuration is used in this paper for comparison with other works. In addition, the novel wrist-to-wrist and wrist-to-finger electrode configurations are evaluated as candidate locations in wearable applications.

### 2.2.1. Chest

Chest, or thoracic, bioimpedance is well studied for impedance cardiography [33] and pneumography [34]. The tetrapolar electrode configuration utilized in this paper was selected to provide a baseline measurement for comparison to other, less-studied configurations. Here, the source current and voltage electrodes are on the left side of the chest, while the sink current and voltage electrodes are on the right side of the chest, resulting in a transverse thoracic measurement. This configuration is similar to configuration D used in [35], and also used in [36,37], which found it to have the highest robustness to noise and the strongest correlation with reference breathing measurements. By sensing the voltage difference closely to the full volume of the lungs and the heart, this configuration gives the largest change in measured impedance for the biological processes of breathing and heart-beat. There are many contributing factors to the changes in measured thoracic impedance [38] over the studied time period (approximately one minute), but the primary factors are respiration [39] and heart activity [33], with studies isolating one of these variables typically requiring suppression of the other [36,40]. A further study of inter-heartbeat changes is available in [41]. Since many other studies have evaluated individual applications, this study focused on the relative changes in complex bioimpedance due to these two processes to further evaluate other electrode configurations.

### 2.2.2. Forearm

Forearm measurements are well studied in the context of breathing [23], blood pressure monitoring [22], and heart rate detection, with multiple papers and avenues of research available. The effect of electrode placement can have a significant impact on the measured impedance [42]. In this context, a tetrapolar electrode configuration centered on the ulnar artery is used, and similar setups can be found in [43,44]. As discussed in [43], the primary short-term time-varying properties in the forearm are blood flow (modulated by heart activity and respiration) and muscle tension. As the arterial wave pulse travels through the measurement area, it is measured by the change in volume and blood impacting the complex impedance of tissue under the electrodes. A further discussion of this measurement

location is available in [22]. In each measurement, the forearm was placed flat on a table with palm up in a relaxed, comfortable position to minimize the effects of muscle tensions and movement. The advantages of a forearm-based measurement system are numerous in the context of remote patient monitoring. A self contained system on the forearm could be relatively hassle-free to the end user. Wrist-based wearables are already common-place, so adding a bioimpedance sensor to existing wrist-based wearables would be highly beneficial. This research extends the range of frequencies described in the existing literature and provides a direct comparison to the chest measurements, enabling an estimation of the comparative sensitivity to respiration and heart activity.

### 2.2.3. Wrist-to-Wrist

Those familiar with segmental bioimpedance spectroscopy [45] recognize that breaking the complex system of the human body into individually measured segments and then adding them together is often more accurate than measuring the entire body at once [46]. However, whole body measurements are still useful and commonly used (due to electrode setup and convenience). In a similar fashion, impedance cardiography and pneumography measured directly on the chest segment of the body will naturally be more diagnostically relevant and accurate than a whole body measurement containing the chest. Wrist-to-wrist measurement are not well characterized in the literature, but have some promising applications in the wearable space where it can be beneficial to trade some measurement fidelity for usability (e.g., smartwatch applications, treadmill, and other fitness applications). We seek to quantify this trade-off so that other researchers can consider using it in future applications, such as watch- or smart clothes- based wearables. The wrist-to-wrist configuration studied here has current electrodes on the wrist close to the palm, and the respective voltage electrodes situated as close as possible to their associated current electrodes. This adds the nearly entire length of the forearm and upper arm on each side of the body to the measured tissue under study. As the chest now makes up a smaller fraction of the measured volume, the change in impedance due to respiration and heart activity will also be smaller.

### 2.2.4. Wrist-to-Finger

The wrist-to-finger configuration is similar to that of the wrist-to-wrist, except that the sink electrodes are placed on the ends of the thumb (voltage sense) and index finger (current sink) of the opposite hand from the source. This configuration is similar to [47] studied for body composition analysis [48], as well as in commercial devices [49,50], and ECG measurements [51]. However, there have not been studies quantifying the effects of respiration and heart activity on the impedance measured in this configuration, which could have an impact on the calculated body composition using this method.

## 2.3. Bioimpedance Sensors and Controllers

To measure bioimpedance, we used two commercially available BioZ integrated controllers with analog front ends. The TI AFE 4300 is used for stimulation frequencies of 8, 16, 32, and 64 kHz, and the MAX30009 is used for all ten frequencies. Each was calibrated by following the calibration procedure in the datasheet. For the AFE 4300, this involved measuring two separate resistors (50 and 100  $\Omega$ ) to calculate the offset and slope. For the Maxim chip, the provided software GUI calibration uses only one resistor (100  $\Omega$ ).

### 2.3.1. AFE 4300

Released in 2012, the TI AFE 4300 [15] has been used in numerous bioimpedance studies since its introduction. It was among the first fully integrated bioimpedance solutions, not requiring an analog front end to be added. This board measures up to 860 samples per second (SPS) through a 14-bit ADC and has a frequency range of 1–255 kHz for FWR (magnitude only) mode. IQ mode is limited to stimulation frequencies of 8, 16, 32, and 64 kHz. In this mode, though, I and Q must be measured alternately, limiting the sample rate to

effectively 430 SPS of both I and Q. This board is primarily sold in a 12 × 12 mm quad flat package.

### 2.3.2. MAX30009

Released in early 2022, the MAXIM MAX30009 BioZ front end has only recently been referenced in the literature [18]. This controller measures up to 4k SPS through a 19-bit ADC across a frequency range of 16–855 kHz. Additionally, this system is capable of simultaneous I and Q measurements, which has advantages for investigations of physiological phenomena requiring fine resolution, such as impedance cardiography. The simultaneous I and Q measurements at all available frequencies is the primary reason that this paper uses the MAX30009 EVKIT for multi-site evaluations. The EVKIT also includes parasitic cancellation traces for high-frequency measurements. Though typical bioimpedance applications stay below 100 kHz due to parasitic capacitance losses [14], these losses are more significant above 500 kHz [52]. The highest frequency used in this paper, 512 kHz, is suitable for a comparison of relative changes, as any parasitic effects will be constant. This controller is primarily sold in a 2 × 2 mm wafer level package.

The MAX30009 bioimpedance controller is an electrical impedance spectroscopy device marketed mainly towards bioimpedance analysis. However, many other applications of the device for general spectral analysis of the complex impedance are possible. The MAX30009 has many features that make it a promising candidate for future studies in complex electrical impedance analysis. According to the datasheet, it can measure complex impedance with frequencies as low as 16 Hz and as high as 806 kHz. While the frequency range may not be quite wide enough for all applications, the lowest available frequency (16 Hz) is lower than many complex impedance analyzers such as the Keysight E4990A, which only measures down to 20 Hz. The high input impedance, low noise paths, and 20 bit ADC result in 17 bits of effective resolution and 0.1% accuracy after calibration. The most attractive feature of this device are the price and size, costing over one hundred times less for a ready to use development kit than comparable impedance analyzers, significantly lowering the barrier to entry for many researchers. A small footprint and small number of external components make it very attractive for low-power embedded sensors and controllers. The advances behind the performance gains and the price to performance ratio improvement for galvanostat systems such as the MAX30009 may lead to further improvements in the potentiostat systems used in electrochemical impedance spectroscopy applications as well as other fields.

### 2.4. Physiological Measurements and Processing

A fine resolution synchronization of BioZ measurements with physiological signals is absolutely necessary to study the changes caused by physiological signals. This study used a custom PPG/ECG sensor MAX 86150 connected to the same microcontroller board as the BioZ module to synchronize our measurements with physiological signals. However, as discussed in [53], this external synchronization is not strictly necessary if the objective is identification of heartbeats and breathing, and a recent paper used only bioimpedance for respiration tracking [54]. The breathing protocol used made possible clear identification of the breath-induced changes in BioZ, and for most locations (except the forearm) the heartbeats are visible as well. The PPG serves to increase confidence in the measurements and provide the possibility for future research to include pulse transit time as a measurement.

All data were processed using MATLAB. Calibration was applied to the bioimpedance signals, which were low-pass filtered at 10 Hz to remove high-frequency noise. The MATLAB function findpeaks was adjusted using reference data to identify peaks due to respiration in one process thread, and peaks due to cardiac activity in another. These data were then windowed into individual breaths or heartbeats, with an offset approximately one second before and after the peaks. For example, with the seven breaths captured at a particular frequency, the peak exhalations were identified and the breaths arranged into a single window where the peak exhalation point was aligned. Then, basic statistics such as

mean, median, and standard deviation could be applied to determine the “average deep breath”. The change in impedance due to a mean deep breath (peak to peak) was divided by the mean of the measurement to determine the relative percent change. A similar procedure was used for the average heartbeat. The bar figures are used throughout the paper to highlight the relative changes in bioimpedance during cardiorespiratory activity between the excitation frequencies. As many studies [36,55] have shown [56], there is a highly linear change in impedance with breathing, which can be used to accurately measure respiration. This study uses a best-case scenario of deep breathing to create the largest average change possible to evaluate the relative change in impedance caused by respiration across multiple frequencies and locations. Visually, as can be seen in the figures throughout this paper, the impedance change due to respiration can be easily identified by the repeating trapezoidal shape, while smaller visual “spikes” may be visible, which correspond to cardiac activity. As an added point of clarification, the reference value for the percent change is variable depending on the frequency as well as the configuration. The percent change is intended to reflect the ease of sensing the activity (respiration or cardiac) at a given electrode configuration and frequency. While the absolute impedance value is an important factor, the higher frequency (above 100 kHz) measurements are impacted by parasitic effects. However, the authors would like to emphasize that any parasitic effects can be considered a constant over the short time period of the measurement (sixty seconds).

### 2.5. BioZ Measurements

For each measurement location, up to 10 frequencies are chosen and measured for at least one minute for each frequency. This gives roughly 7 breaths and an average of 65 heartbeats in the sample space to compare frequencies against. With 512 SPS for the MAX30009, this gives roughly 30,000 samples for comparison. With 200 SPS for AFE4300 IQ mode, there are roughly 12,000 samples. The MAX30009 sensor was set to use 64 microAmps of current. The amplifier range and bandwidth were both set to “high”. The voltage mode amplitude (RMS) was set to 354 mV. All onboard filtering was set to bypass.

### 2.6. Subjects

In this pilot study, we evaluated the sensitivity of signals at candidate locations and excitation frequencies for the monitoring of respiration and heart activity in wearable applications. Since each combination of electrode location and excitation frequency requires a statistically significant number of respiration cycles, in our cases, sixty seconds, the objective of this pilot study is to assess promising combinations of electrode locations and excitation frequencies for follow-up studies. The bioimpedance measurements were taken on a single male subject, age 28, height 71 inches, weight 165 lbs. Reference distance measurements included chest circumference—38 inches (full inhalation), 35.5 inches (full exhalation). Wrist circumference—6.5 inches. Wrist-to-wrist distance: 55 inches.

### 2.7. Protocols

For each measurement, the area was cleaned with alcohol and allowed to dry before the electrodes were applied. 3M Red Dot 2560 Ag/AgCl electrodes were used for connection to the body. A web-based program [57] was used to indicate the breathing pattern to the user. This program displayed a two second inhale, four second hold, and two second exhale repeating pattern. Bioimpedance-only identification of breathing is also used in [54]. The effect of this breathing pattern is an easily identifiable trapezoidal pattern in the measured impedance. Measuring for one minute ensures that at least seven breaths are captured.

## 3. Results

This section presents the relative changes in impedance components across frequencies for all measurement locations, separated into changes due to heart activity and changes due to respiration.

### 3.1. Chest Measurements

Chest measurements of bioimpedance are widely used to monitor breathing. Figure 2 shows a representative sample of one full recording of a bioimpedance measurement for the chest location at 128 kHz. Here, the repeating patterns of impedance increase with inhalation, constant with breath hold, and decrease with exhalation represent the change in impedance corresponding to respiration, while the smaller spike-like variations show the change corresponding to individual heartbeats. The magnitude component of the impedance, Figure 2a, is dominated by changes corresponding to respiration, while changes corresponding to heart activity are relatively more visible in the phase, Figure 2b. The phenomenon of visible changes corresponding to heart activity in the phase component were found to occur primarily at 128 kHz and above. We present relative changes caused by breathing and heart activity for different locations suitable for wearable monitoring in the sections below.

#### 3.1.1. Heartbeats

The relative change in measured bioimpedance caused by cardiac activity is presented in Figure 3. The figure shows the relative change (y-axis) of the magnitude, Figure 3a, phase Figure 3b, real part, Figure 3c, and imaginary part, Figure 3d, of the impedance across 10 candidate frequencies (x-axis). Here, the relative change in most categories is highest in very low frequencies and frequencies of 64 kHz or above. The highest relative changes are in the imaginary and phase components.

#### 3.1.2. Respiration

Relative change in measured impedance corresponding to the average deep breath (discussed in Section 2.4) as measured on the chest is shown in Figure 4. The figure shows the relative change (y-axis) of the magnitude, Figure 4a, phase, Figure 4b, real part, Figure 4c, and imaginary part, Figure 4d, of the impedance across 10 candidate frequencies (x-axis). Generally, the changes are consistent across frequencies, but there is a smaller change in the frequencies of 2–16 kHz.

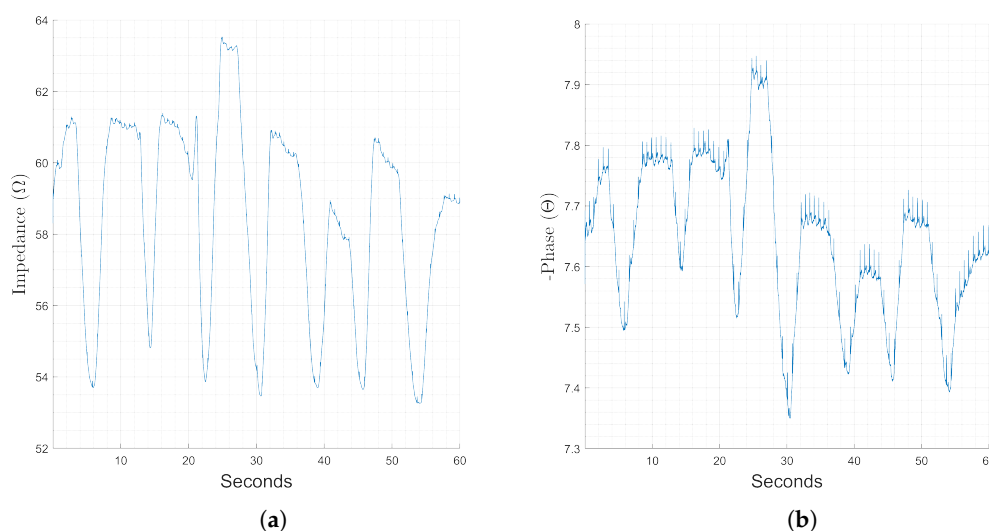


**Figure 2.** Changes in the magnitude (a) and phase (b) components of recorded bioimpedance at the chest location. The stimulation frequency used was 128 kHz and the recording time was 60 s.



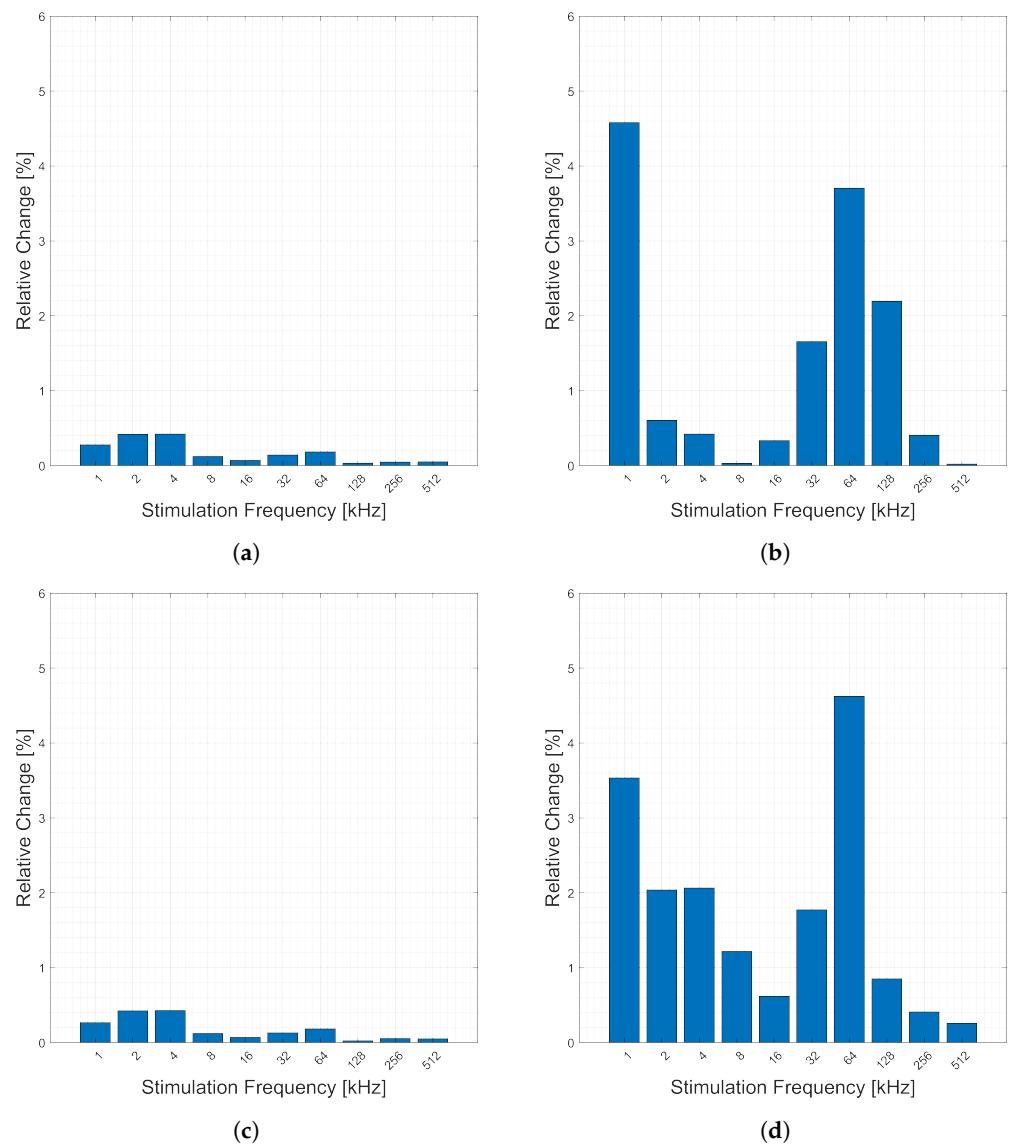


**Figure 3.** Relative changes in the (a) magnitude, (b) phase, (c) real, and (d) imaginary components of bioimpedance corresponding to heart activity measured across the chest for selected frequencies.

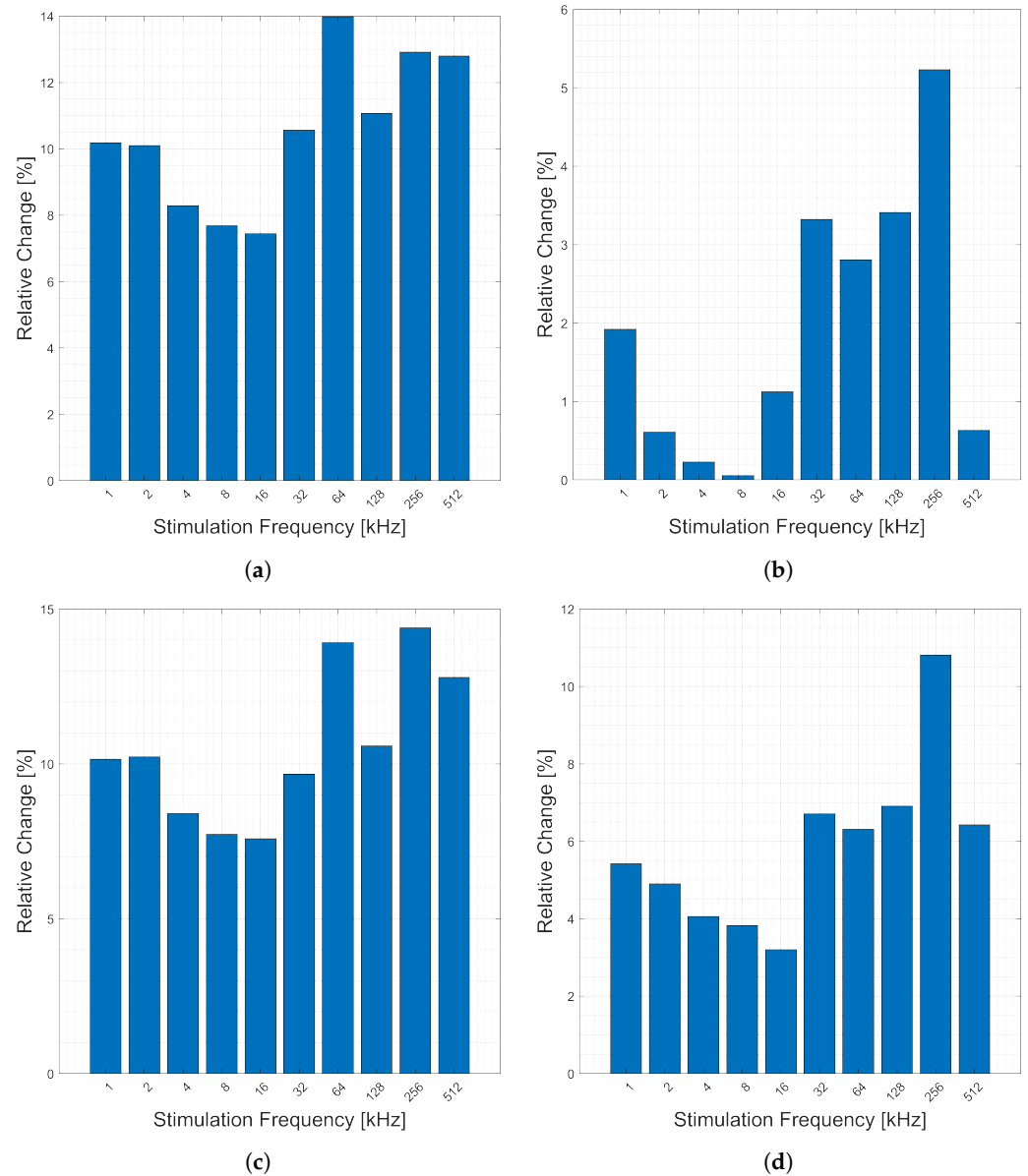


**Figure 4.** Relative changes in the (a) magnitude, (b) phase, (c) real, and (d) imaginary components of bioimpedance corresponding to respiration measured across the chest for selected frequencies.

### 3.2. Forearm Measurements

Forearm measurements are commonly used in research studies for respiratory and heart activity monitoring. Figure 5 below presents a representative sample of a full sixty second measurement with a stimulation frequency of 8 kHz on the forearm. Here, the magnitude representation, Figure 5a, has no clear trends, but the phase, Figure 5b, shows clear changes corresponding to heart activity in the form of small spikes corresponding to arterial pulsing as well as to respiration in the form of the mild trapezoidal modulation. In this section, the evaluated stimulus frequencies are all strong candidates for monitoring heart activity, though increasing the stimulation frequency showed slightly higher percent changes in the phase.

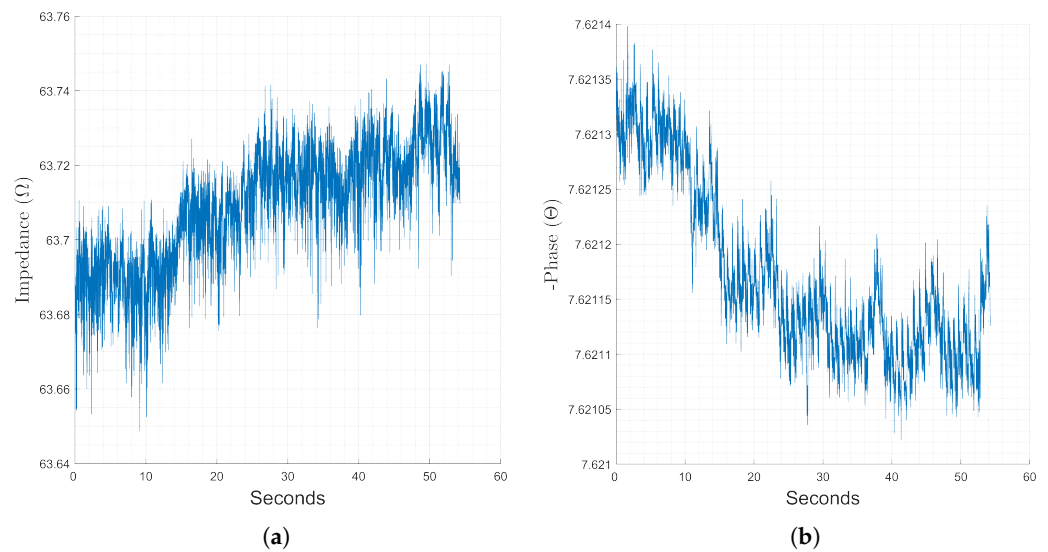


**Figure 5.** Changes in the magnitude (a) and phase (b) components of recorded bioimpedance at the forearm location, stimulation frequency of 64 kHz recorded for 60 s.

### 3.2.1. Heart Activity

The measurements corresponding to heart activity for the forearm are presented in Figure 6. There are consistent relative changes (y-axis) across all stimulation frequencies for the magnitude, Figure 6a, real, Figure 6c, and imaginary, Figure 6d, parts of the impedance. However, the phase, Figure 6b, change increases with frequency (x-axis), though it is still a small relative change. This is due to the absolute value of the real part decreasing relative to the imaginary part, causing a larger relative change in phase with increasing frequency.

### 3.2.2. Respiration

Presented in Figure 7 are the relative changes (y-axis) corresponding to respiration at various stimulation frequencies (x-axis). Similar to the heartbeats, there are higher relative changes in the phase, Figure 7b, due to the decreased magnitude of the real part relative to the imaginary part. With the exception of the phase, there is a consistent change across all frequencies for respiratory activity measured at the forearm. Only the imaginary part, Figure 7d, exceeds 0.1% change, for three stimulation frequencies.

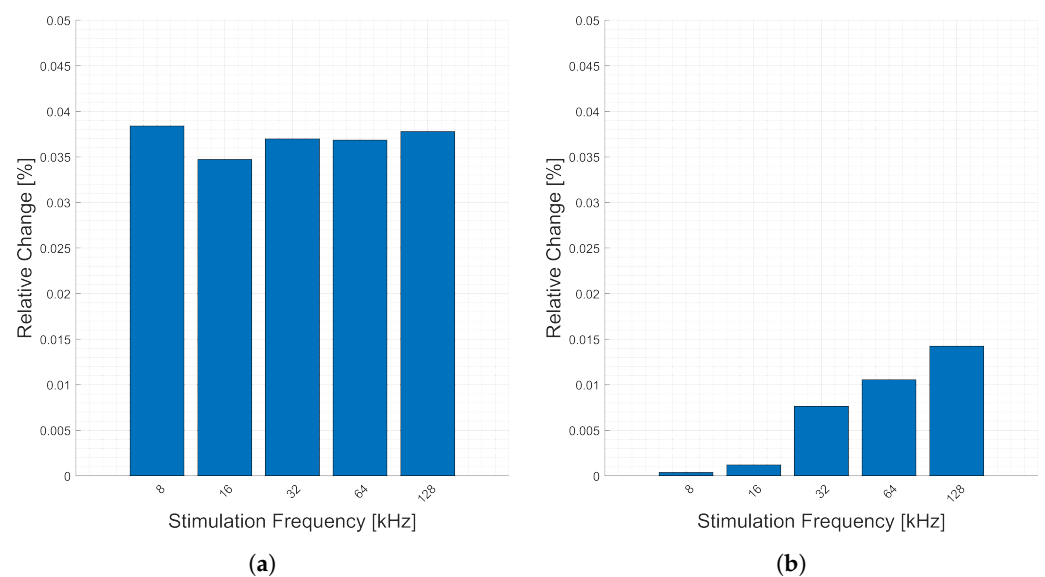


**Figure 6.** Cont.

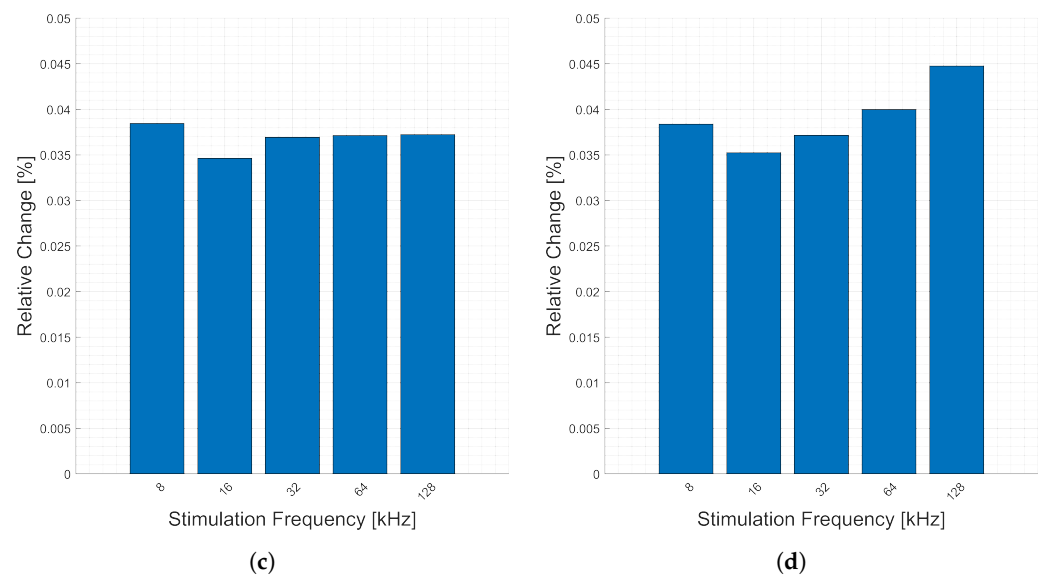


**Figure 6.** Relative changes in the (a) magnitude, (b) phase, (c) real, and (d) imaginary components of bioimpedance corresponding to heart activity measured on the forearm measured for selected frequencies.

### 3.3. Wrist-to-Wrist

Measurement with the novel wrist-to-wrist measurement location are presented in this section. A representative sample of a sixty second recording at this location with a stimulation frequency of 2 kHz is presented in Figure 8. The magnitude component of the impedance, Figure 8a, is dominated by the trapezoidal changes corresponding to respiratory activity, though heart activity is visible as a small sinusoidal variation. Changes in the phase component, Figure 8b, correspond strongly with respiration. For this section, AFE4300 results are added at 8, 16, and 32 kHz.

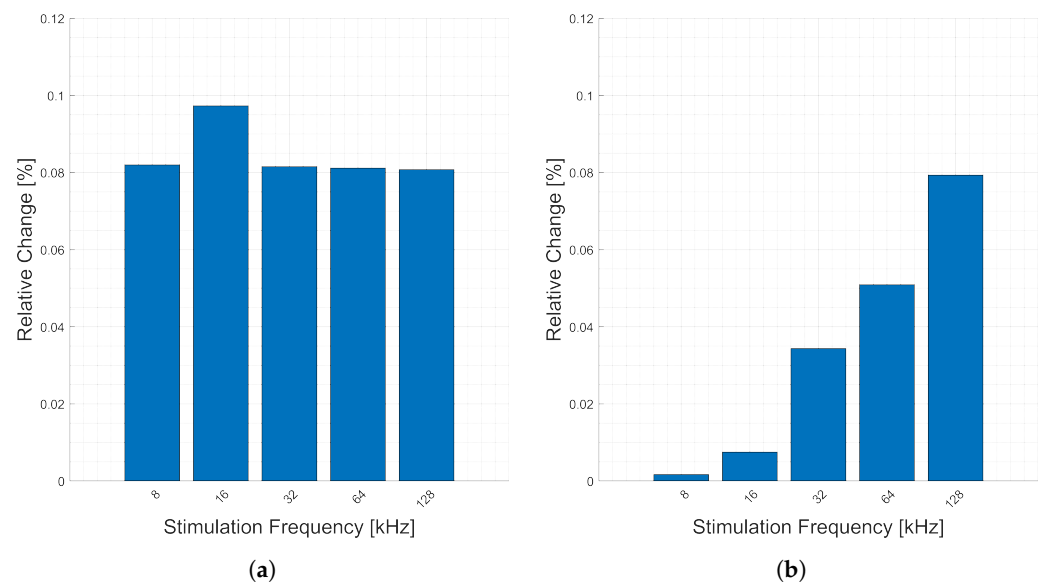


**Figure 7.** Cont.

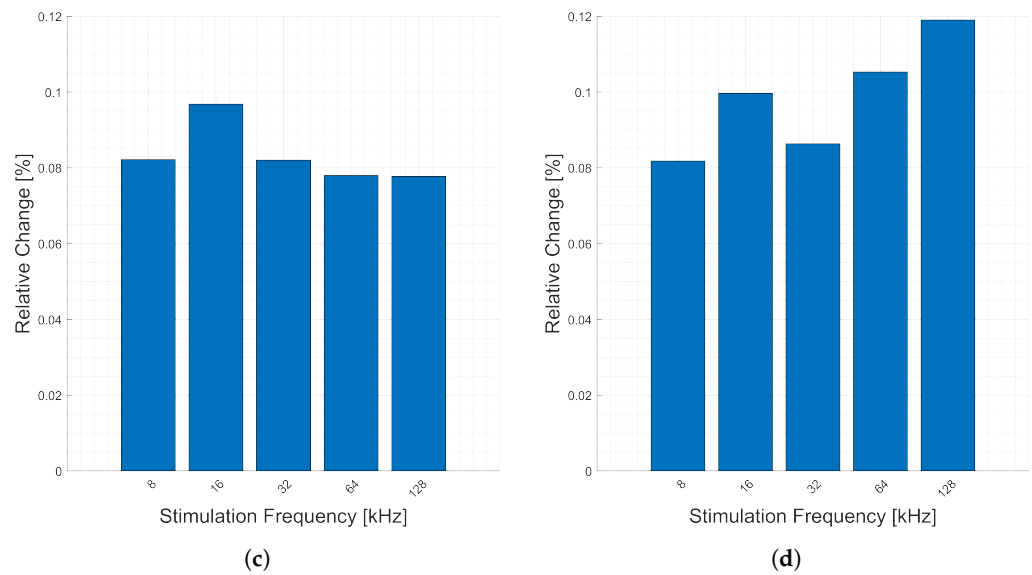


**Figure 7.** Relative changes in the (a) magnitude, (b) phase, (c) real, and (d) imaginary components of bioimpedance corresponding to respiration measured on the forearm for selected frequencies.

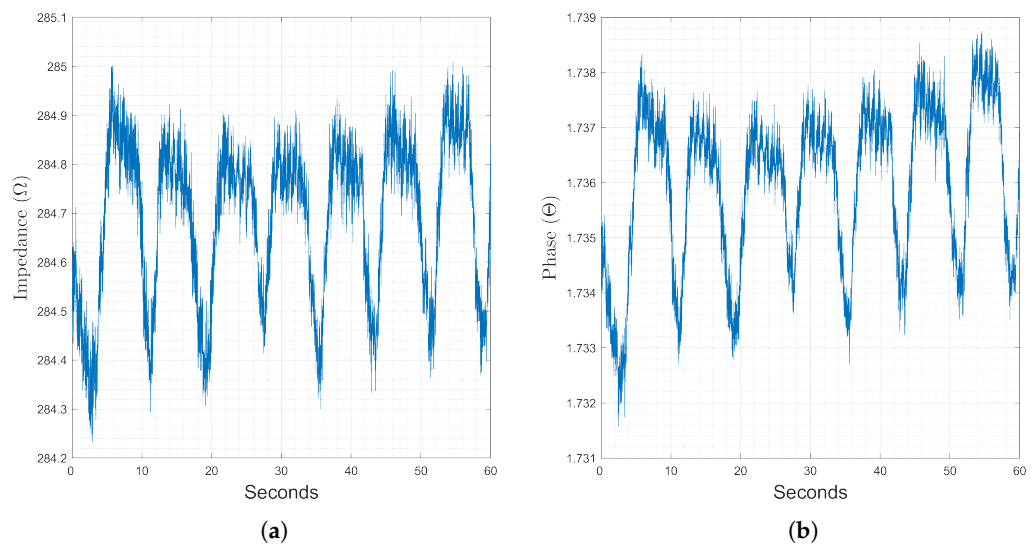


**Figure 8.** Changes in the magnitude (a) and phase (b) components of recorded bioimpedance at the wrist-to-wrist location, stimulation frequency of 2 kHz recorded for 60 seconds.

### 3.3.1. Heart Activity

The relative changes (y-axis) in the magnitude, Figure 9a, phase, Figure 9b, real, Figure 9c, and imaginary, Figure 9d, components of bioimpedance corresponding to heart activity for the wrist-to-wrist sensing location are presented in Figure 9. The highest relative changes occur in stimulation frequencies (x-axis) between 32 and 128 kHz. The frequencies above 32 kHz have an average change of nearly double that of frequencies below 32 kHz, though 8 kHz shows a stronger response than 1–4 kHz and 16 kHz. The AFE 4300 measurements provided a similar response, but only for 8, 16, and 32 kHz.

### 3.3.2. Respiration

The relative changes (y-axis) corresponding to respiration are presented in Figure 10. Generally, the relative change increases with higher stimulation frequencies (x-axis). The frequencies above 8 kHz have an average change of nearly double that of frequencies below 8 kHz in all components, except for phase. The AFE 4300 measurements provided a similar response for the breathing, but only for 8, 16, and 32 kHz.

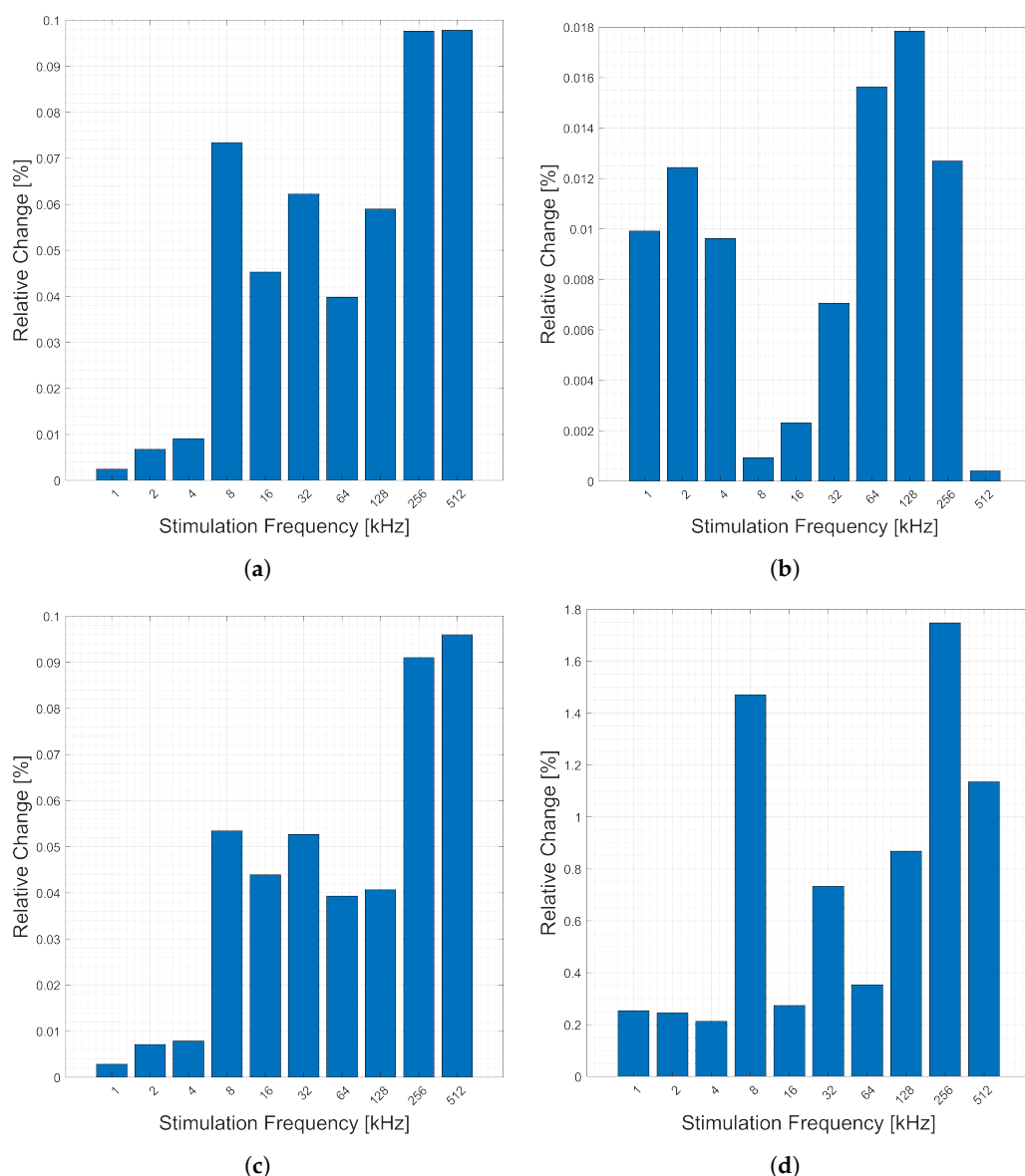


**Figure 9.** Relative changes in the (a) magnitude, (b) phase, (c) real, and (d) imaginary components of bioimpedance corresponding to heart activity measured across the body from left wrist to right wrist for selected frequencies.

### 3.4. Wrist-to-Fingers

Measurements taken with the novel wrist-to-finger electrode configuration are presented in this section. A representative time series measurement is presented in Figure 11. Similar to the chest measurements, the changes corresponding to respiratory activity are clearly identified by the trapezoidal pattern in the magnitude component, Figure 11a, while the changes corresponding to heart activity are less visible. The phase component, Figure 11b, shows clear heart activity, and some weakly correlated changes with breathing.

#### 3.4.1. Heart Activity

The relative changes (y-axis) due to heart activity measured from one wrist to the opposite side index finger is presented in Figure 12. Note that stimulation frequency 256 kHz is missing (data corruption). Generally, lower stimulation frequencies (x-axis) have higher relative changes in all components. The large change in the imaginary component is due to the smaller absolute value of this component, relative to the other components, Figure 12.

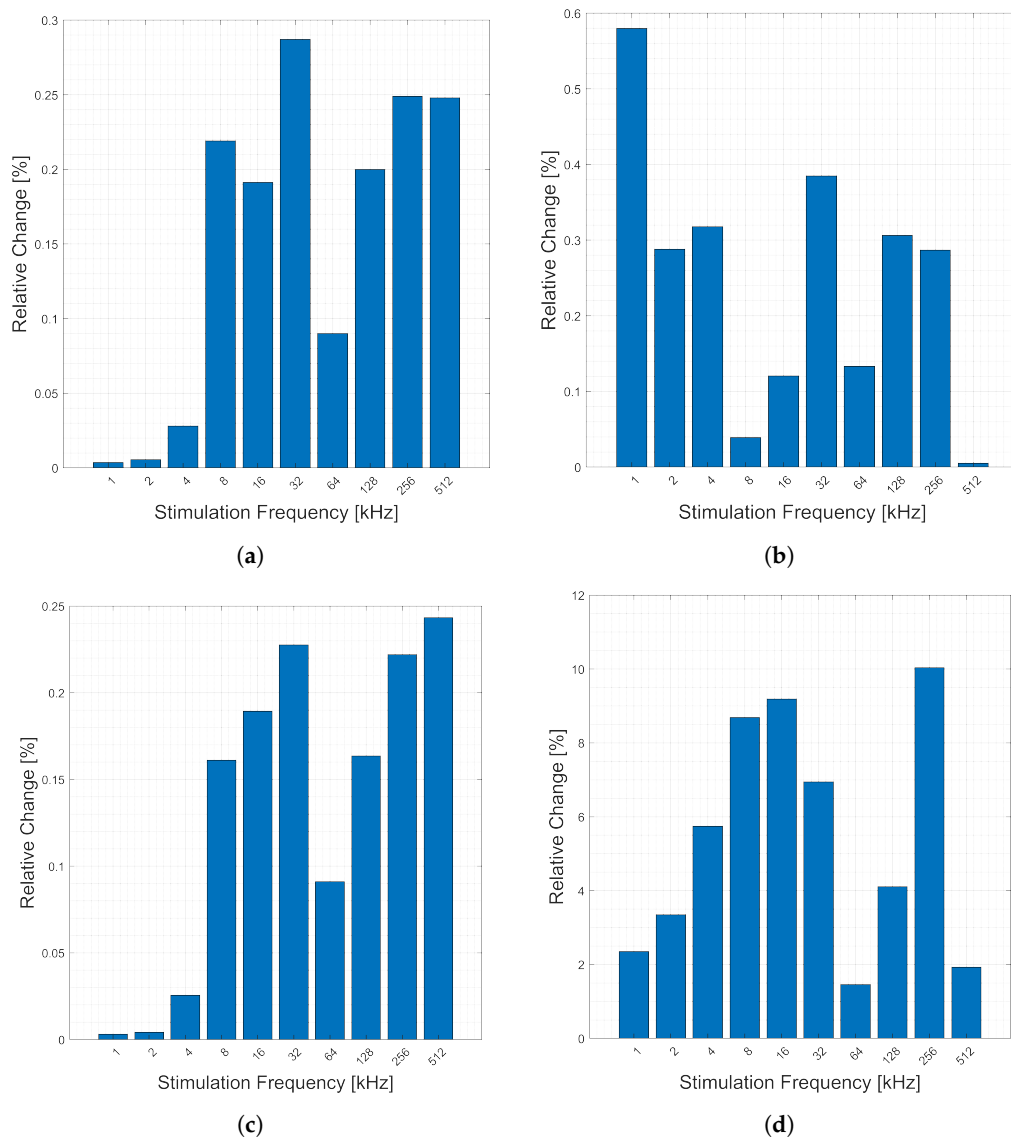


**Figure 10.** Relative changes in the (a) magnitude, (b) phase, (c) real, and (d) imaginary components of bioimpedance corresponding to respiration measured across the body from left wrist to right wrist for selected frequencies.

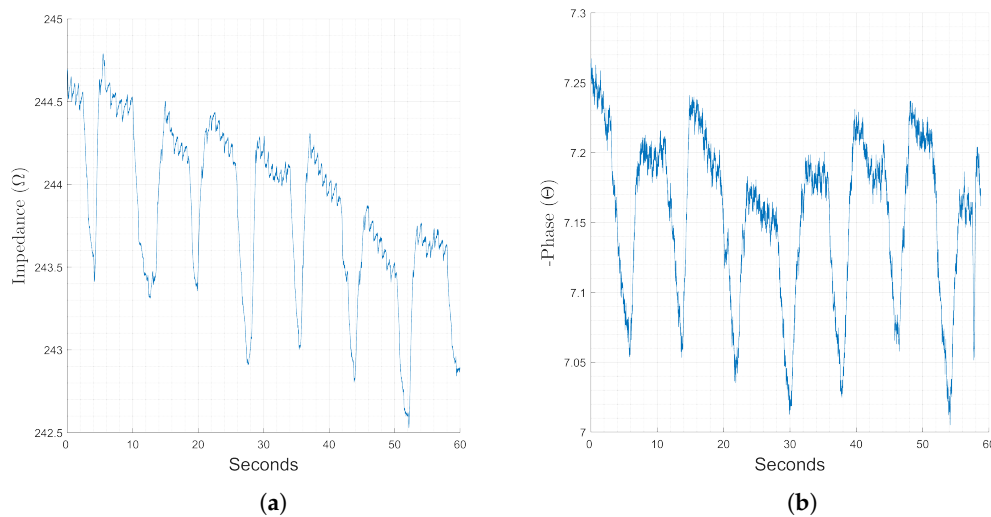


**Figure 11.** Changes in the magnitude (a) and phase (b) components of recorded bioimpedance at the wrist-to-finger location, stimulation frequency 64 kHz recorded for 60 seconds.

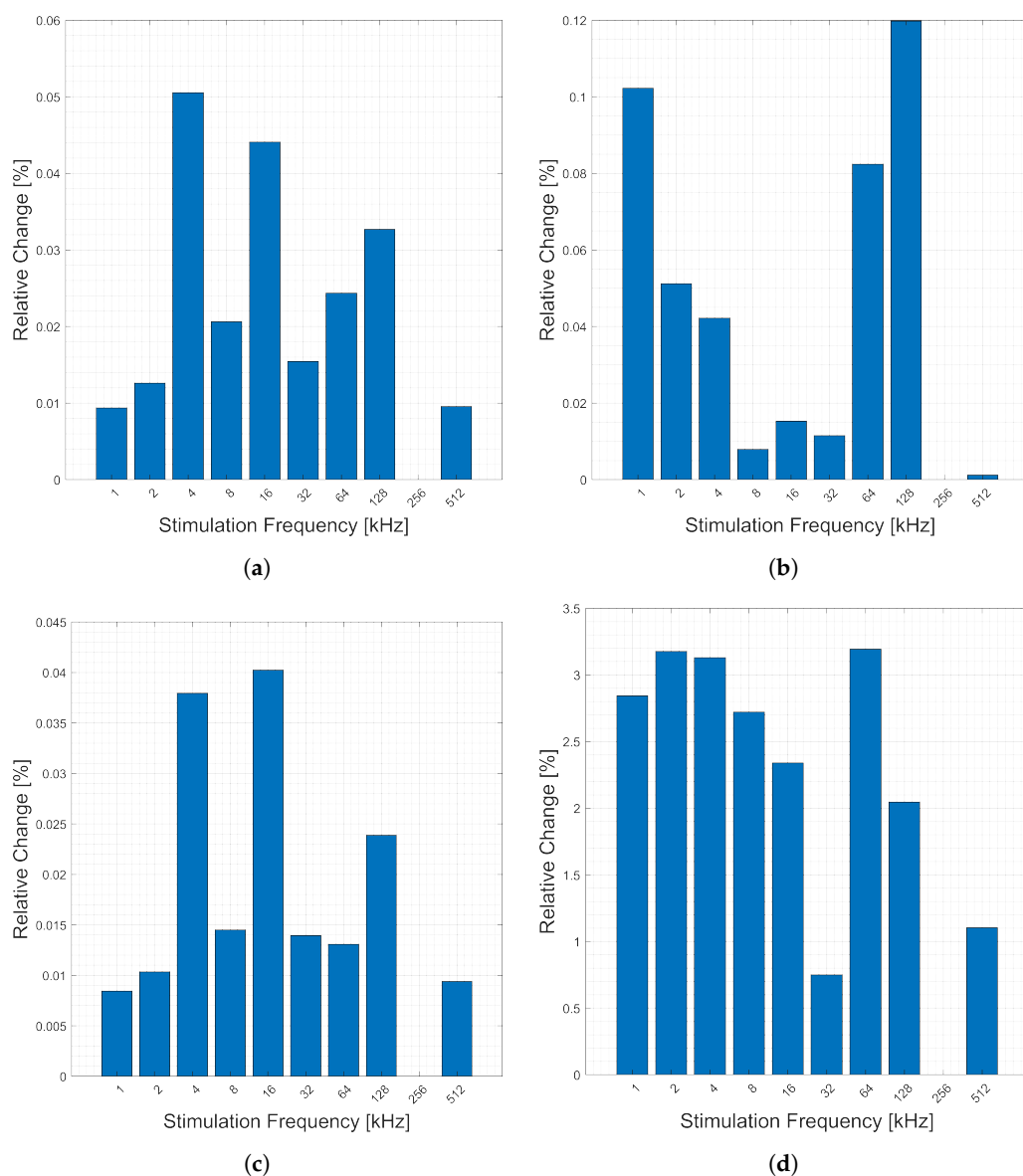


**Figure 12.** Relative changes in the (a) magnitude, (b) phase, (c) real, and (d) imaginary components of bioimpedance corresponding to heart activity measured across the body from left wrist to right thumb and forefinger for selected frequencies.

### 3.4.2. Respiration

Figure 13 shows the relative changes (y-axis) corresponding to respiration between stimulation frequencies (x-axis) for this location. Note that frequency 256 kHz is missing (data corruption). There seem to be no clear trends in the frequencies in this location. The relative change in the imaginary component is larger than that of the real, but the overall magnitude of it is much smaller.



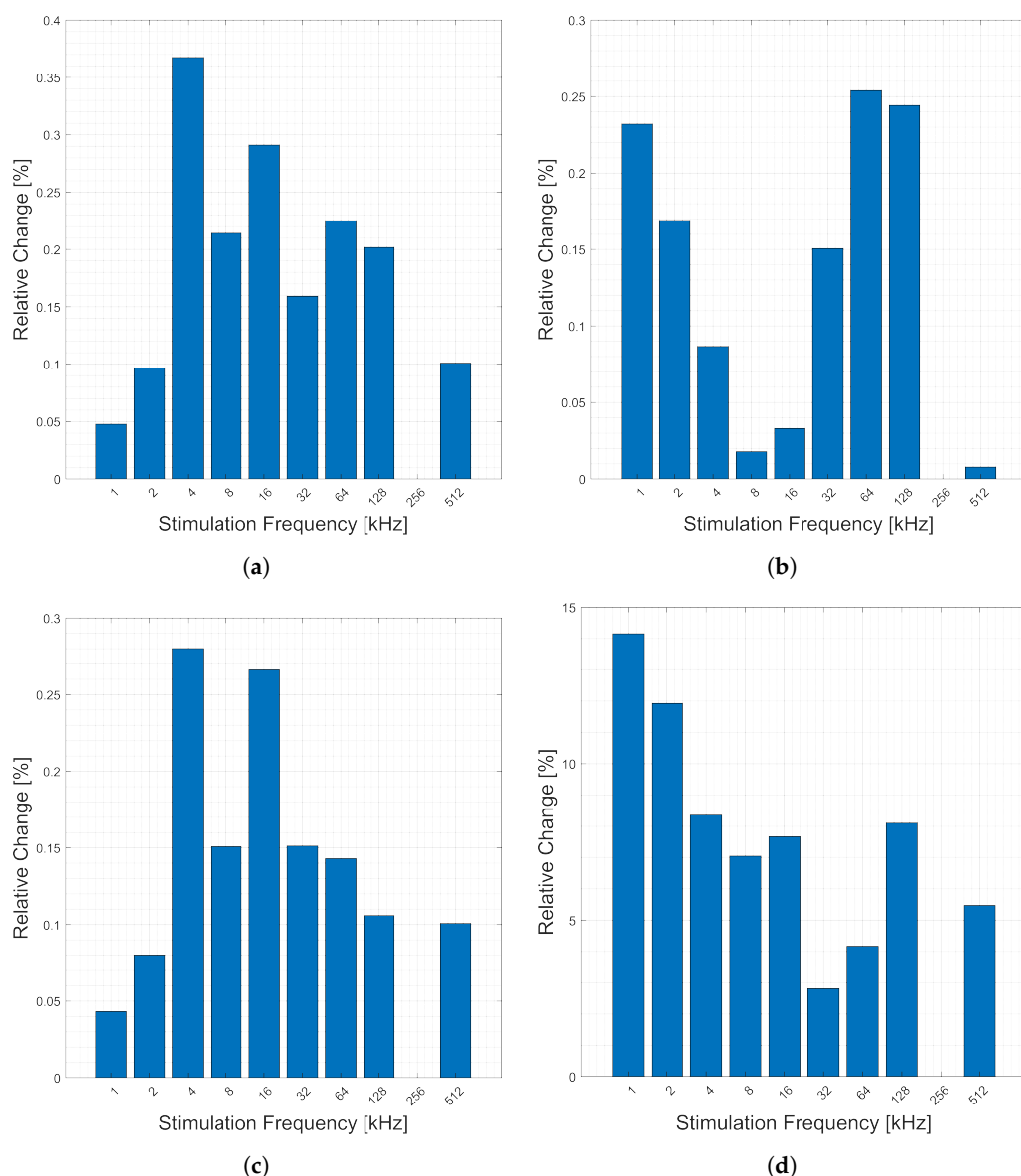


**Figure 13.** Relative changes in the (a) magnitude, (b) phase, (c) real, and (d) imaginary components of bioimpedance corresponding to respiration measured across the body from left wrist to right thumb and forefinger for selected frequencies.

#### 4. Discussion

In this paper, methods and locations suitable for the wearable monitoring of vital signs using changes of complex bioimpedance were evaluated. Physiological signals of interest include deep breathing and cardiac activity. The investigation was based on two COTS controllers, the TI AFE4300 and MAX30009, where a subset of the measurements were performed with the AFE4300. The two evaluated devices provide similar accuracy and impedance results in the overlapping frequency range. The TI AFE4300 is limited to stimulation frequencies of 8, 16, 32, and 64 kHz in (non-simultaneous) IQ mode (the magnitude-only stimulation frequencies are much higher). The MAX30009, however, can use any frequency within the range of 1–860 kHz with simultaneous I and Q measurements and has significantly lower power consumption and a smaller PCB footprint. The MAX30009 is nearly a decade newer than the AFE4300, so this increased performance is not necessarily a surprise. We concluded that the MAX30009 is an excellent candidate for future studies of wearable sensors. The extended frequency range as well as simultaneous I and Q measurements provide the option to evaluate changes in magnitude, phase, resistive,

and reactive components in one measurement. The relative changes of BioZ across multiple tetrapolar electrode configurations and stimulation frequencies were characterized to identify the best use cases for the combination of frequency and electrode configuration for the given wearable application.

(17% at 64 kHz, 0.5% at 256 kHz, respectively), on the forearm (0.098% at 16 kHz, 0.04% at 8 kHz), wrist-to-wrist across the body (0.28% at 256 kHz, 0.04% at 256 kHz, respectively), and wrist-to-finger across the body (0.35% at 4 kHz, 0.05% at 4 kHz, respectively). By measuring directly at the source, chest measurements have the highest sensitivity to the biological processes of breathing and heart activity, with an average change in magnitude of 12% across all surveyed frequencies for breathing and 0.5% for heart activity. Peak relative changes in magnitude for this measurement location were recorded as 17% at 64 kHz for breathing and 0.5% at 256 kHz for heartbeats. These values are within the expected range for chest-based measurements. As expected, the measurement locations further away from the chest decreased in measurement sensitivity, but might be feasible for certain wearable applications. At the forearm, for instance, the average change due to respiration and heart activity decreased to 0.098% and 0.04%, respectively. The forearm represents an indirect measurement of these parameters. The wrist-to-wrist across the body measurements have changes of 0.25% and 0.015%, respectively, nearly an order of magnitude higher than the forearm measurement. Similarly, the wrist-to-finger measurements have changes of 0.2% and 0.03%, slightly lower than the wrist-to-wrist measurement, but higher than the forearm measurements. Although absolute values change between measurement setups, the short term relative change in impedance is stable and 0.1–1% change is significant on the short time scale relevant for physiological measurements.

The phase may be a more reliable indicator of heart and lung activity than the magnitude in some applications, as shown by the forearm measurements as well as high-frequency (above 100 kHz) chest measurements, which is a novel finding. We find that, generally, the imaginary component has a higher relative change due to its lower relative magnitude. The relative changes for the wrist-to-wrist and wrist-to-finger configurations were roughly an order of magnitude smaller than the chest measurement. However, this decrease in sensitivity may be acceptable for monitoring applications that need lower resolution or can tolerate occasional missed measurement during continuous monitoring. As an example, an existing wrist-worn body composition measurement device, such as the Samsung Galaxy Watch 4, may be able to be used for intermittent measurements of respiration and heart activity. Additionally, a theoretical wearable with continuous forearm-based measurements used for long term monitoring combined with intermittent wrist-to-wrist or wrist-to-finger measurements for reference and/or calibration may have significant advantages for remote patient monitoring applications. A guided deep breathing routine during simultaneous wrist-to-(finger or wrist) and forearm measurements could provide a user-specific calibration for both measurements, enabling at-home respiration monitoring for at-risk and low-mobility patients.

The biggest limitation of this study is the small sample size. While we minimized the time between measurements, postural changes between measurements could induce small changes in the absolute value of the impedance measured. Future studies need additional subjects to confirm these findings. Future studies would do well to consider additional frequencies that are traditionally not used in bioimpedance, such as those above 100 kHz, when researching physiological phenomena such as respiration and cardiac activity that vary on short time scales.

An important finding of this paper was that deep breathing and heartbeats may influence bioimpedance measurements in the studied whole-body measurement configurations. There may be variations of nearly 0.5% in measured impedance due to the phase of the breathing cycle at the time of measurement, and this variation changes with each excitation frequency. Simple averaging may not be sufficient to account for these variations without special consideration of the frequency spectra of the underlying processes. This can lead to errors in assessed body composition as well as intra- and extra-cellular water and

other Cole-dispersion-related variables. Applications that use other components of the impedance may be impacted as well if they include the chest in the tissue under study. The actual change in body composition parameters or the assessment error in body composition depends on the algorithm and frequencies used in a given device or monitor. To demonstrate these effects, we have given the data collected in the wrist-to-wrist sensing configuration as a Cole–Cole plot, shown in Figure 14, with frequencies of 8, 16, 32, 50, 64, 100, and 128 kHz. These changes shown in the Cole–Cole plot demonstrate the magnitude of the effect of respiration, where each real and imaginary pair are shifted up and to the right for every frequency. Note that the changes here are with a deep breath, not a normal breath, which would result in a smaller change. There are multiple papers on sources of error with BIS measurements, but we were unable to find papers in the open literature that describe this change as a contributing source of error. Our intent was to inform the research community of this lesser-known source of potential error in body composition measurement. It may also enable new applications of traditional body composition equipment, if the change in estimated body composition is strongly correlated with lung volume. Our preliminary testing on a Withings Body+ body composition weight scale indicated a change of approximately 0.2% in estimated body fat percentage and total body water with full vs. empty lungs. We emphasize the need to consider the phase of breathing during the assessment of body composition in wearable health monitoring applications.

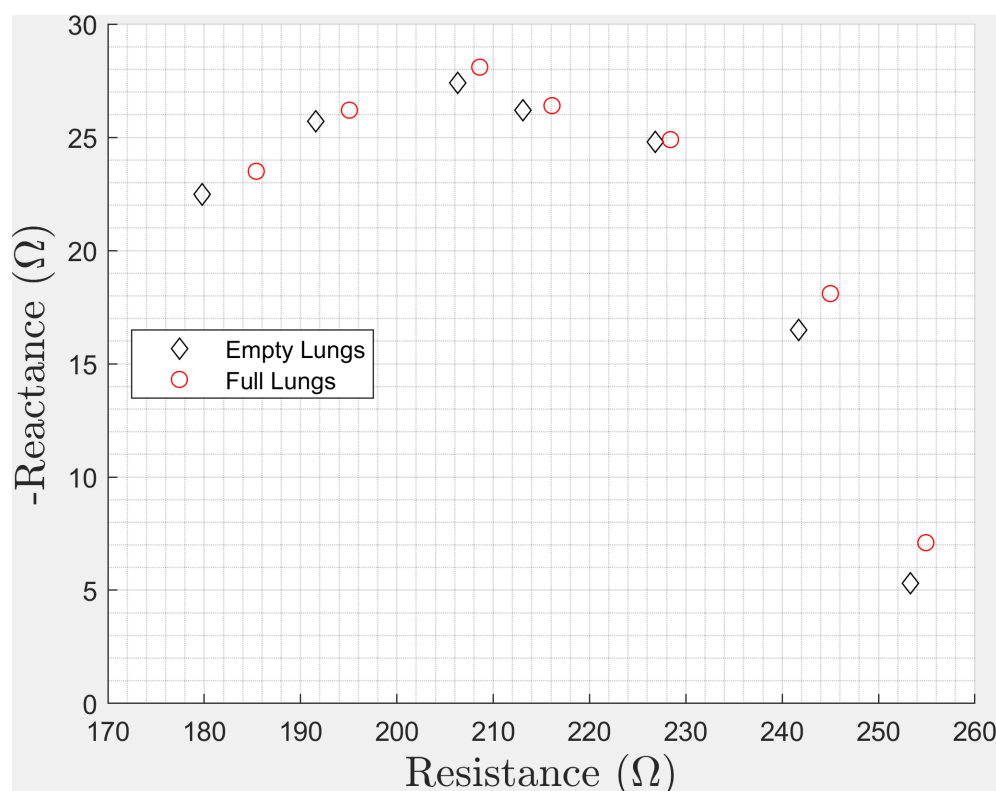


**Figure 14.** A Cole–Cole plot with the frequencies of 8, 16, 32, 50, 64, 100, 128 kHz measured in the wrist-to-wrist electrode configuration. Here the pairs of diamonds (black) and circles (red) show the change in measured impedance due to respiration at a given frequency.

This study addressed a gap in the literature for bioimpedance-enabled remote patient monitoring and wearable applications. Four bioimpedance sensing locations and ten measurement frequencies were assessed. This study is unique due to the evaluation of two novel sensing locations in comparison with others and the use of a commercially available bioimpedance controller to enhance the repeatability of the study, as well as the wide frequency range studied. Many other studies cover multiple electrode locations, but typically use only one frequency, or use custom hardware. We observed that the

relative change in wrist-to-wrist and wrist-to-finger measurements of respiratory and heart activity compared favorably with forearm measurements for respiration and heart activity applications. The presented results represent signal characteristics for a limited number of subjects used in this study; however, they represent guidance for promising configurations and measurement frequencies for follow-up studies using larger populations or specific conditions. We believe that the presented results may provide guidance for designers of wearable sensors for experimental and deployment setup.

**Author Contributions:** Conceptualization, R.J.M.; methodology, R.J.M. and E.J.; software, R.J.M.; validation, R.J.M. and E.J.; formal analysis, R.J.M.; investigation, R.J.M.; resources, R.J.M.; data curation, R.J.M.; writing—original draft preparation, R.J.M.; writing—review and editing, R.J.M. and E.J.; visualization, R.J.M.; supervision, E.J. All authors have read and agreed to the published version of the manuscript.

**Funding:** This research received no external funding.

**Institutional Review Board Statement:** The study was conducted in accordance with the Declaration of Helsinki, and approved by the Institutional Review Board (or Ethics Committee) of University of Alabama in Huntsville (EE202284, 5 December 2022).

**Informed Consent Statement:** Informed consent was obtained from all subjects involved in the study.

**Data Availability Statement:** The data presented in this study are available on request from the corresponding author.

**Conflicts of Interest:** The authors declare no conflict of interest.

## References

1. Lukaski, H.C. Evolution of bioimpedance: A circuitous journey from estimation of physiological function to assessment of body composition and a return to clinical research. *Eur. J. Clin. Nutr.* **2013**, *67*, S2–S9. [CrossRef]
2. Heymsfield, S.; Heshka, S.; Allison, D.; Pierson, R. *Body Composition*; Henry Stewart Talks: London, UK, 2009.
3. Norman, K.; Stobäus, N.; Pirlich, M.; Bosy-Westphal, A. Bioelectrical phase angle and impedance vector analysis—Clinical relevance and applicability of impedance parameters. *Clin. Nutr.* **2012**, *31*, 854–861. [CrossRef]
4. Oppliger, R.A.; Bartok, C. Hydration testing of athletes. *Sports Med.* **2002**, *32*, 959–971.
5. Tattersall, J. Bioimpedance Analysis in Dialysis: State of the Art and What We Can Expect. *Blood Purif.* **2009**, *27*, 70–74. [CrossRef]
6. Davies, S.J.; Davenport, A. The role of bioimpedance and biomarkers in helping to aid clinical decision-making of volume assessments in dialysis patients. *Kidney Int.* **2014**, *86*, 489–496.
7. Moshkovitz, Y.; Kaluski, E.; Milo, O.; Vered, Z.; Cotter, G. Recent developments in cardiac output determination by bioimpedance: comparison with invasive cardiac output and potential cardiovascular applications. *Curr. Opin. Cardiol.* **2004**, *19*, 229–237. [PubMed]
8. Di Somma, S.; De Berardinis, B.; Bongiovanni, C.; Marino, R.; Ferri, E.; Alfei, B. Use of BNP and bioimpedance to drive therapy in heart failure patients. *Congest. Heart Fail.* **2010**, *16*, S56–S61. [PubMed]
9. Impedimed. SFB7. Available online: <https://www.impedimed.com/products/research-devices/sfb7/> (accessed on 16 January 2023).
10. Fu, B.; Freeborn, T.J. Residual impedance effect on emulated bioimpedance measurements using Keysight E4990A precision impedance analyzer. *Measurement* **2019**, *134*, 468–479. [CrossRef]
11. Jaffrin, M.Y.; Morel, H. Body fluid volumes measurements by impedance: A review of bioimpedance spectroscopy (BIS) and bioimpedance analysis (BIA) methods. *Med. Eng. Phys.* **2008**, *30*, 1257–1269.
12. Di Vincenzo, O.; Marra, M.; Scalfi, L. Bioelectrical impedance phase angle in sport: A systematic review. *J. Int. Soc. Sports Nutr.* **2019**, *16*, 49.
13. Piccoli, A.; Pastori, G.; Codognotto, M.; Paoli, A. Equivalence of information from single frequency v. bioimpedance spectroscopy in bodybuilders. *Br. J. Nutr.* **2007**, *97*, 182–192. [PubMed]
14. Scharfetter, H.; Hartinger, P.; Hinghofer-Szalkay, H.; Hutten, H. A model of artefacts produced by stray capacitance during whole body or segmental bioimpedance spectroscopy. *Physiol. Meas.* **1998**, *19*, 247. [PubMed]
15. TI.com. AFE4300 Data Sheet, Product Information and Support. Available online: <https://www.ti.com/product/AFE4300> (accessed on 29 September 2022).
16. Carrasco-Marginet, M.; Castizo-Olier, J.; Rodríguez-Zamora, L.; Iglesias, X.; Rodríguez, F.A.; Chaverri, D.; Brotons, D.; Irurtia, A. Bioelectrical impedance vector analysis (BIVA) for measuring the hydration status in young elite synchronized swimmers. *PLoS ONE* **2017**, *12*, e0178819. [CrossRef]
17. Anisimov, A.A.; Belov, A.V.; Sergeev, T.V.; Sannikova, E.E.; Markelov, O.A. Evolution of Bioamplifiers: From Vacuum Tubes to Highly Integrated Analog Front-Ends. *Electronics* **2022**, *11*, 2402. [CrossRef]

18. Crandall, H.; Burt, A.; Sanchez, B. Characterization of the Analog Device Inc (ADI) MAX30009 Bioimpedance Analog Front End Chip. In Proceedings of the 2022 44th Annual International Conference of the IEEE Engineering in Medicine & Biology Society (EMBC), Scotland, UK, 11–15 July 2022; pp. 2502–2505. ISSN 2694–0604. [[CrossRef](#)]
19. Maxim Integrated. MAX30009 Low-Power, High-Performance Bioimpedance Analog Front-End. Available online: <https://www.maximintegrated.com/en/products/sensors/MAX30009.html#tech-docs> (accessed on 29 September 2022).
20. Zurich Instruments. MFIA 500 kHz/5 MHz Impedance Analyzer. Available online: <https://www.zhinst.com/en/products/mfia-impedance-analyzer> (accessed on 28 September 2022).
21. Adans-Dester, C.P.; Bamberg, S.; Bertacchi, F.P.; Caulfield, B.; Chappie, K.; Demarchi, D.; Erb, M.K.; Estrada, J.; Fabara, E.E.; Freni, M.; et al. Can mHealth Technology Help Mitigate the Effects of the COVID-19 Pandemic? *IEEE Open J. Eng. Med. Biol.* **2020**, *1*, 243–248. [[CrossRef](#)]
22. Ibrahim, B.; Jafari, R. Cuffless Blood Pressure Monitoring from an Array of Wrist Bio-Impedance Sensors Using Subject-Specific Regression Models: Proof of Concept. *IEEE Trans. Biomed. Circuits Syst.* **2019**, *13*, 1723–1735. [[CrossRef](#)]
23. Sel, K.; Ibrahim, B.; Jafari, R. ImpediBands: Body Coupled Bio-Impedance Patches for Physiological Sensing Proof of Concept. *IEEE Trans. Biomed. Circuits Syst.* **2020**, *14*, 757–774. [[CrossRef](#)]
24. Piuze, E.; Pisa, S.; Pittella, E.; Podestà, L.; Sangiovanni, S. Wearable belt with built-in textile electrodes for cardio-respiratory monitoring. *Sensors* **2020**, *20*, 4500.
25. Berkebile, J.A.; Mabrouk, S.A.; Ganti, V.G.; Srivatsa, A.V.; Sanchez-Perez, J.A.; Inan, O.T. Towards estimation of tidal volume and respiratory timings via wearable-patch-based impedance pneumography in ambulatory settings. *IEEE Trans. Biomed. Eng.* **2021**, *69*, 1909–1919.
26. Pino, E.J.; Gómez, B.; Monsalve, E.; Aqueveque, P. Wireless Low-Cost Bioimpedance Measurement Device for Lung Capacity Screening. In Proceedings of the 2019 41st Annual International Conference of the IEEE Engineering in Medicine and Biology Society (EMBC), Berlin, Germany, 23–27 July 2019; pp. 1187–1190. ISSN 1558-4615. [[CrossRef](#)]
27. Nicolò, A.; Massaroni, C.; Schena, E.; Sacchetti, M. The Importance of Respiratory Rate Monitoring: From Healthcare to Sport and Exercise. *Sensors* **2020**, *20*, 6396. [[CrossRef](#)]
28. Bertemes-Filho, P.; Morcelles, K.F. Wearable Bioimpedance Measuring Devices. In *Medicine-Based Informatics and Engineering*; Springer: Berlin/Heidelberg, Germany, 2022; pp. 81–101.
29. Dutt, A.G.; Verling, M.; Karlen, W. Wearable bioimpedance for continuous and context-aware clinical monitoring. In Proceedings of the 2020 42nd Annual International Conference of the IEEE Engineering in Medicine & Biology Society (EMBC), Montreal, QC, Canada, 20–24 July 2020; pp. 3985–3988.
30. Buttorff, C.; Ruder, T.; Bauman, M. *Multiple Chronic Conditions in the United States*; RAND Corporation: Santa Monica, CA, USA, 2017. [[CrossRef](#)]
31. Hajat, C.; Stein, E. The global burden of multiple chronic conditions: A narrative review. *Prev. Med. Rep.* **2018**, *12*, 284–293. [[CrossRef](#)]
32. DeVore, A.D.; Wosik, J.; Hernandez, A.F. The Future of Wearables in Heart Failure Patients. *JACC Heart Fail.* **2019**, *7*, 922–932. [[CrossRef](#)]
33. Bour, J.; Kellett, J. Impedance cardiography—A rapid and cost-effective screening tool for cardiac disease. *Eur. J. Intern. Med.* **2008**, *19*, 399–405. [[CrossRef](#)]
34. Pacela, A.F. Impedance pneumography—A survey of instrumentation techniques. *Med. Biol. Eng.* **1966**, *4*, 1–15. [[CrossRef](#)]
35. Wang, H.B.; Yen, C.W.; Liang, J.T.; Wang, Q.; Liu, G.Z.; Song, R. A Robust Electrode Configuration for Bioimpedance Measurement of Respiration. *J. Healthc. Eng.* **2014**, *5*, 313–328. [[CrossRef](#)]
36. Seppä, V.P.; Hyttinen, J.; Viik, J. A method for suppressing cardiogenic oscillations in impedance pneumography. *Physiol. Meas.* **2011**, *32*, 337–345. [[CrossRef](#)]
37. Logic, J.; Maksud, M.; Hamilton, L. Factors affecting transthoracic impedance signals used to measure breathing. *J. Appl. Physiol.* **1967**, *22*, 251–254. [[PubMed](#)]
38. Petroianni, A. Cardiopulmonary Function Interactions during Noninvasive Mechanical Ventilation: Key Topics and Clinical Implications. In *Noninvasive Mechanical Ventilation: Theory, Equipment, and Clinical Applications*; Esquinas, A.M., Ed.; Springer International Publishing: Berlin/Heidelberg, Germany, 2016; pp. 7–19. [[CrossRef](#)]
39. Grenvik, A.; Ballou, S.; McGinley, E.; Millen, J.E.; Cooley, W.L.; Safar, P. Impedance Pneumography: Comparison between Chest Impedance Changes and Respiratory Volumes in 11 Healthy Volunteers. *Chest* **1972**, *62*, 439–443. [[CrossRef](#)]
40. Ernst, J.M.; Litvack, D.A.; Lozano, D.L.; Cacioppo, J.T.; Berntson, G.G. Impedance pneumography: Noise as signal in impedance cardiography. *Psychophysiology* **1999**, *36*, 333–338. [[CrossRef](#)]
41. Gaw, R.L. The Effect of Red Blood Cell Orientation on the Electrical Impedance of Pulsatile Blood with Implications for Impedance Cardiography. Ph.D. Thesis, Queensland University of Technology, Brisbane, Australia, 2010.
42. Fu, B.; Freeborn, T.J. Estimating Localized Bio-Impedance with Measures from Multiple Redundant Electrode Configurations. In Proceedings of the 2018 40th Annual International Conference of the IEEE Engineering in Medicine and Biology Society (EMBC), Honolulu, HI, USA, 18–21 July 2018; pp. 4351–4354. ISSN 1558-4615. [[CrossRef](#)]
43. Yu, Y.; Anand, G.; Lowe, A.; Zhang, H.; Kalra, A. Towards Estimating Arterial Diameter Using Bioimpedance Spectroscopy: A Computational Simulation and Tissue Phantom Analysis. *Sensors* **2022**, *22*, 4736. [[CrossRef](#)]

44. Anand, G.; Lowe, A. Investigating Electrical Impedance Spectroscopy for Estimating Blood Flow-Induced Variations in Human Forearm. *Sensors* **2020**, *20*, 5333. [[CrossRef](#)] [[PubMed](#)]
45. Bracco, D.; Thiebaud, D.; Chiolero, R.L.; Landry, M.; Burckhardt, P.; Schutz, Y. Segmental body composition assessed by bioelectrical impedance analysis and DEXA in humans. *J. Appl. Physiol.* **1996**, *81*, 2580–2587. [[CrossRef](#)]
46. Pateyjohns, I.R.; Brinkworth, G.D.; Buckley, J.D.; Noakes, M.; Clifton, P.M. Comparison of three bioelectrical impedance methods with DXA in overweight and obese men. *Obesity* **2006**, *14*, 2064–2070. [[CrossRef](#)] [[PubMed](#)]
47. Jung, M.H.; Namkoong, K.; Lee, Y.; Koh, Y.J.; Eom, K.; Jang, H.; Jung, W.; Bae, J.; Park, J. Wrist-wearable bioelectrical impedance analyzer with miniature electrodes for daily obesity management. *Sci. Rep.* **2021**, *11*, 1238. [[CrossRef](#)] [[PubMed](#)]
48. AURA Strap. Available online: <https://auradevices.io/strap> (accessed on 28 September 2022).
49. Samsung US. Galaxy Watch4 Classic Smartwatch. Available online: <https://www.samsung.com/us/watches/galaxy-watch4-classic/> (accessed on 28 September 2022).
50. Galaxy Watch5 Smartwatch | Samsung US. Available online: <https://www.samsung.com/us/watches/galaxy-watch5/> (accessed on 28 September 2022).
51. Apple Watch Series 8. Available online: <https://www.apple.com/apple-watch-series-8/> (accessed on 28 September 2022).
52. Mathews, R.J.; Freeborn, T.J. Modeling and experimental validation of parasitic capacitance effects on emulated bioimpedance measurements with high-impedance residuals. *Int. J. Circuit Theory Appl.* **2020**, *48*, 1057–1069. [[CrossRef](#)]
53. Krivoshei, A.; Kukk, V.; Min, M. Decomposition method of an electrical bio-impedance signal into cardiac and respiratory components. *Physiol. Meas.* **2008**, *29*, S15–S25. [[CrossRef](#)]
54. Blanco-Almazán, D.; Groenendaal, W.; Lijnen, L.; Önder, R.; Smeets, C.; Ruttens, D.; Catthoor, F.; Jané, R. Breathing Pattern Estimation Using Wearable Bioimpedance for Assessing COPD Severity. *IEEE J. Biomed. Health Inform.* **2022**, *26*, 5983–5991 [[CrossRef](#)]
55. Blanco-Almazán, D.; Groenendaal, W.; Lozano-García, M.; Estrada-Petrocelli, L.; Lijnen, L.; Smeets, C.; Ruttens, D.; Catthoor, F.; Jané, R. Combining Bioimpedance and Myographic Signals for the Assessment of COPD During Loaded Breathing. *IEEE Trans. Biomed. Eng.* **2021**, *68*, 298–307. [[CrossRef](#)]
56. Blanco-Almazán, D.; Groenendaal, W.; Catthoor, F.; Jané, R. Chest movement and respiratory volume both contribute to thoracic bioimpedance during loaded breathing. *Sci. Rep.* **2019**, *9*, 1–11.
57. Anti-Stress Maximum Relaxation Breathing Pacer. Available online: <https://www.grc.com/breathe.htm> (accessed on 7 October 2022).

**Disclaimer/Publisher’s Note:** The statements, opinions and data contained in all publications are solely those of the individual author(s) and contributor(s) and not of MDPI and/or the editor(s). MDPI and/or the editor(s) disclaim responsibility for any injury to people or property resulting from any ideas, methods, instructions or products referred to in the content.